

# EXPLORING THE EFFICACY AND LIMITATIONS OF SHOCK-COOLING MODELS: NEW RESULTS FOR TYPE II SUPERNOVAE OBSERVED BY THE KEPLER MISSION

ADAM RUBIN AND AVISHAY GAL-YAM

Department of Particle Physics and Astrophysics, Weizmann Institute of Science, 234 Herzl St., Rehovot, Israel

*Draft version May 17, 2022*

## ABSTRACT

Shock-cooling models provide robust predictions for the early time emission from core-collapse SNe. Modern surveys have begun discovering and following SNe shortly after first light—providing first measurements of the rise of Type II SNe. We explore how shock cooling models can constrain the progenitor’s radius, explosion velocity, and local host extinction. We fit synthetic photometry in several realistic observing scenarios and find that ultraviolet observations can constrain the progenitor’s radius to a statistical uncertainty of  $\pm 10 - 15\%$ , with a systematic uncertainty of  $\pm 20\%$ . With these observations the local host extinction can be constrained to  $\pm 0.05$  mag and the velocity to  $\pm 5\%$  with a systematic uncertainty of  $\pm 10\%$ . We also re-analyze the SN light curves presented in Garnavich et al. (2016) and find that KSN 2011a can be fit by a blue supergiant model with a progenitor radius of  $R_s = 10^{+37(\text{stat})+8(\text{sys})}_{-7(\text{stat})-1(\text{sys})} R_\odot$ , while KSN 2011d can be fit with a red supergiant model with a progenitor radius of  $R_s = 140^{+91(\text{stat})+23(\text{sys})}_{-47(\text{stat})-28(\text{sys})} R_\odot$ . Our results do not agree with those of Garnavich et al. (2016). Moreover, we re-evaluate their claims and find that there is no statistically significant evidence for shock breakout in the light curve of KSN 2011d.

## 1. INTRODUCTION

Modern surveys such as the Palomar Transient Factory (PTF, iPTF; Law et al. 2009; Kulkarni 2013) and the Panoramic Survey Telescope & Rapid Response System (PanSTARRS; Kaiser et al. 2002) have successfully been discovering and following SNe close to their date of first light. In addition to a handful of individual objects (Pastorello et al. 2006; Quimby et al. 2007; Gezari et al. 2008; Schawinski et al. 2008; Gal-Yam et al. 2011; Arcavi et al. 2011; Ergon et al. 2014; Valenti et al. 2014; Bose et al. 2015; Gall et al. 2015; Arcavi et al. 2016; Tartaglia et al. 2016), samples with good coverage during the rise of Type II SNe have only recently been published (Rubin et al. 2016). Garnavich et al. (2016, G16) published two SNe discovered in the Kepler mission data. These are extremely well sampled SN II LCs and we address them in this paper.

In parallel, theorists have developed models to describe the expected early-time emission from core-collapse SNe. Waxman et al. (2007) and Nakar & Sari (2010, NS10) derived similar models describing the post-shock envelope emission from massive envelopes. Rabinak & Waxman (2011, RW11) extended the theory to non-constant opacity, and improved the calculation of the color temperature by taking into account bound-free absorption which was previously neglected. This subject has been recently revisited. Sapir & Waxman (2016, SW16) re-derived the analytical results for constant opacity, and extended the theory to later times for low-mass envelopes. Shussman et al. (2016) explored calibrating analytical models against numerically simulated explosions and progenitors. Each of these theories depends explicitly (or implicitly) on the following assumptions:

1. The ejecta has expanded sufficiently such that it

adam.rubin@weizmann.ac.il

is no longer planar and must be considered in the spherical geometry.

2. The emission is from a very thin shell which was initially near the edge of the star and the photosphere has penetrated only a small fraction of the ejected mass.
3. The temperature is above 0.7 eV and recombination effects are not important.

For massive envelopes, the temperature typically drops below 0.7 eV before any appreciable depth has been reached. This is especially true for progenitors with small radii where adiabatic losses are significant.

While NS10 and RW11/SW16 roughly agree on the bolometric luminosity in the spherical phase, RW11 and SW16 included bound-free (the dominant) absorption in the calculation of the color temperature. This can have a dramatic effect on the estimation of the progenitor’s radius, and leads us to use SW16 in this paper. For a more thorough discussion see SW16 Section 1.

Several recent works (González-Gaitán et al. 2015; Gall et al. 2015; Garnavich et al. 2016) compared to such models, but did not properly consider their limits of validity. Rubin et al. (2016) showed that including data beyond the model’s validity range leads to incorrect assessment of the uncertainties and potentially to the acceptance of models which should be rejected.

Here we simulate data and explore the potential of shock-cooling models to constrain the progenitor’s radius, the explosion velocity, and the local host extinction under various observing programs with various facilities. We also revisit the G16 Kepler SNe and re-analyze the data while taking into account the limitations of the models and their uncertainties.

## 2. THE MODEL

In this work we use the recent derivation for constant opacity of SW16. SW16 extended the previous models for low-mass envelopes, where the photosphere penetrates the envelope before the temperature has dropped below 0.7 eV. They found an approximation for extending the light curve (LC) after equation 2 (Section 1) no longer holds, which depends on the density structure of the star. In this work we study massive hydrogen envelopes, therefore we use the unextended model.

The two equations which we use are for the photospheric temperature and bolometric luminosity. They are given in SW16 (their equation 4) and are reproduced here:

$$T_{ph} = 1.61 [1.69] \left( \frac{v_{s8.5} t_d^2}{f_\rho M_0 \kappa_{0.34}} \right)^{\epsilon_1} \frac{R_{13}^{1/4}}{\kappa_{0.34}^{1/4}} t_d^{-1/2} \text{ eV} \quad (1)$$

$$L = 2.0 [2.1] \times 10^{42} \left( \frac{v_{s8.5} t_d^2}{f_\rho M_0 \kappa_{0.34}} \right)^{-\epsilon_2} \frac{v_{s8.5} R_{13}}{\kappa_{0.34}} \frac{\text{erg}}{\text{s}} \quad (2)$$

where  $\kappa = 0.34 \kappa_{0.34} \text{ cm}^2 \text{ g}^{-1}$ ,  $v_{s*} = 10^{8.5} v_{s8.5} \text{ cm s}^{-1}$ ,  $M = 1 M_0 M_\odot$ ,  $R = 10^{13} R_{13} \text{ cm}$ ,  $\epsilon_1 = 0.027 [0.016]$ , and  $\epsilon_2 = 0.086 [0.175]$  for  $n = 3/2$  [3].

The period of validity of the model is given by

$$t > 0.2 \frac{R_{13}}{v_{s8.5}} \max \left[ 0.5, \frac{R_{13}^{0.4}}{(f_\rho \kappa_{0.34} M_0)^{0.2} v_{s8.5}^{0.7}} \right] \text{ d} \quad (3)$$

$$t < 3 f_\rho^{-0.1} \frac{\sqrt{\kappa_{0.34} M_0}}{v_{s8.5}} \text{ d} \quad (4)$$

where the first limit describes the requirement for sufficient expansion (spherical phase) and the second limit describes the requirement that the photosphere has only penetrated a small fraction of the envelope's mass. Additionally, to ensure fully ionized hydrogen we require

$$t < \arg(T_{ph}(t) = 0.7 \text{ eV}) \quad (5)$$

The specific flux is given by

$$f_\lambda = \frac{L_{bol}}{4\pi R_{ph}^2} \frac{T_{col}}{hc} g_{BB} \left( \frac{hc}{\lambda T_{col}} \right) \quad (6)$$

where  $R_{ph}$  is the photospheric radius,  $T_{col}$  is the color temperature, and  $g_{BB}$  is the dimensionless black body function given by

$$g_{BB}(x) = \frac{15}{\pi^4} \frac{x^5}{e^x - 1} \quad (7)$$

SW16 explored numerically several different progenitors with varying core to mantle mass ratios and found that the density normalization  $f_\rho = 1 - 3 [0.1 - 0.8]$  for  $n = 3/2$  [3] respectively (assuming normal stars with core to mantle mass ratios of  $0.1 - 1$ , SW16 Figure 5). Here we take  $f_\rho = 1 [0.1]$  for  $n = 3/2$  [3] respectively, appropriate for a core to mantle mass of 1. However the emission is weakly dependent on  $f_\rho$ . SW16 also show that the ratio of the color temperature to the photospheric temperature is well behaved and given by  $T_{col}/T_{ph} = 1.1 [1.0] \pm 0.025 [0.05]$  for  $n = 3/2$  [3] (SW16 Figures 11 and 13). We use these nominal values. See

TABLE 1  
PARAMETERS USED IN THE  
SYNTHETIC DATA

	RSG	BSG
$z$	0.02	0.0075
DM	34.76	32.61
$n$	3/2	3
$\kappa$	0.34	0.34
$R_s/R_\odot$	500.0	50.0
$f_\rho$	1.0	0.1
$T_{col}/T_{ph}$	1.1	1.0
$v_{s8.5}$	1.0	1.0
$A_V$	0.1	0.1
$R_V$	3.1	3.1

Section 3.3 and Figure 1 for the effect of these systematic uncertainties on the inferred parameters.

### 3. FITTING SYNTHETIC DATA

In order to estimate the efficacy of shock-cooling models we simulated a synthetic photometry campaign. We explored discovery in R-band roughly 0.5 days after explosion with follow-up triggered one day later. We synthesized the following followup scenarios: photometry in Bessell (1990) BVRI, UBVRI, or UBVRI + *SWIFT/UVOT* with a one day cadence. To ensure these followup scenarios are realistic, we matched them to the observational campaign of SN 2013fs (Valenti et al. 2016, Yaron et al. 2016 in press). SN 2013fs was discovered just hours after its estimated explosion and was studied with an aggressive campaign both from the ground and from space with *SWIFT/UVOT*. We simulated two SNe with red supergiant (RSG) and blue supergiant (BSG) progenitors, and sampled the models with the same cadence and filters as SN 2013fs was observed.

In order to explore what may be achieved with future UV facilities, we also simulated the expected photometry from ULTRASAT (Sagiv et al. 2014). ULTRASAT is a proposed UV satellite observatory which will acquire high cadence (15 minute) UV photometry at 2500Å. We simulated UBVRI + ULTRASAT with 1 hour cadence and pre-explosion photometry (a conservative scenario given the 15 minute cadence design). We note that, the dependence of  $T_{col}/T_{ph}$  on the progenitor's structure introduces systematic uncertainties which are larger than the statistical uncertainties in the cases we considered. Improvement in the model, stellar evolution codes, and observations may help to reduce these systematic uncertainties.

We generated synthetic data from SW16 equation 4 using the parameters in Table 1. The extinction for each central wavelength was calculated using the Cardelli et al. (1989) prescription. Different redshifts were chosen for both models such that they gave roughly the same observed peak magnitude ( $m_{peak} \sim 17 - 18$ ). All magnitudes reported here are in the AB system unless stated otherwise. The distance modulus was calculated using Planck Collaboration et al. (2015) cosmology with  $H_0 = 67.74$ ,  $\Omega_m = 0.31$ ,  $\Omega_\Lambda = 0.69$ .

#### 3.1. Noise model

To get a realistic model of the noise we adopted 5% uncertainties for all filters. The limiting magnitude in the

TABLE 2  
FILTER PARAMETERS USED.

Filter	Effective wavelength (Å)	Limiting magnitude
UVW2	2229.9	22.75
UVM2	2262.1	22.0
UVW1	2677.1	21.75
U	3605.0	22.0
B	4413.0	22.0
V	5512.1	22.0
R	6585.9	22.0
I	8059.8	22.0
ULTRASAT	2500.0	22.0

ground based observations was consistently  $\sim 22$  magnitudes, for UVOT we took the average limiting magnitude of the actual observations. The effective wavelengths and limiting magnitudes used in this work are summarized in Table 2. We converted the limiting magnitude to a flux error  $\sigma_b$  and used the following equation to generate noise for the model.

$$\sigma^2 = \sigma_b^2 + (0.05f)^2 \quad (8)$$

where  $f$  is the model flux. We then drew the synthetic observations from a normal distribution with mean  $f$  and variance  $\sigma^2$ .

### 3.2. Fitting procedure

Fitting NS10/RW11/SW16 models with a simple log-likelihood test statistic is non-trivial, because the limitations of validity require including different data points in each fit. One possible solution, which is not satisfactory, is to limit the analysis to a specific window of time. This approach was taken in Rubin et al. (2016); Valenti et al. (2014); Bose et al. (2015). While this guarantees that all of the explored models are valid in the window, it does not take into account that the models must be valid over *their* entire range of validity (including data points outside the chosen window). We solve this problem by considering the P-value of each fit. The process is as follows:

- Choose a set of model parameters
- Calculate the time range of validity given the parameters
- Calculate the P-value using

$$P = 1 - \text{CDF}(\chi^2, \nu) \quad (9)$$

where CDF is the cumulative distribution function,  $\chi^2$  is the value of the chi-squared statistic of the fit, and  $\nu$  is the number of degrees of freedom (including only those data points which are within the time range of validity).

In this way we can ensure that the accepted fits are *fully self-consistent*. We defined the critical value to be  $\text{P-value} > 5\%$ . This means that there is less than a 5% chance that the data came from a rejected model.

We generated models on a grid of  $v_{88.5}$ ,  $R_s$ ,  $A_V$ . For each point on the multi-dimensional grid we calculated the  $\chi^2$  statistic taking into account only those data points

which were at times when the model is valid. Note that there is a dependence on  $M_{ej}$ , and  $f_\rho$  through the small pre-factors in equations 1. We discuss these in Section 3.3.

### 3.3. Systematic uncertainties

SW16 models depend to some degree on underlying assumptions of the stellar structure. This appears through two parameters,  $M_{ej}$  and  $f_\rho$ , which weakly affect the results through the exponents  $\epsilon_1$  and  $\epsilon_2$  in equations 1 and 2. In addition, the predicted band luminosity depends on the color temperature and its relation to the photospheric temperature. This dependence is degenerate between  $R$  and  $v_{88.5}$ . This is because the photospheric temperature depends on  $R^{1/4}$  and is practically independent of  $v_{88.5}$ , while the bolometric luminosity goes like  $v_{88.5}^2 R$ . We evaluated the systematic uncertainties by exploring how the best fit parameters depend on the values of  $T_{col}/T_{ph}$ ,  $f_\rho$  and  $M_{ej}$ . The results are shown in Figure 1. For each case we studied we fit the model to the extreme cases of the systematic uncertainties in  $T_{col}/T_{ph}$ , and  $f_\rho$ . We report the most extreme best fit values for the radius and velocity as the systematic uncertainties. The ejected mass can in principle be constrained from observations. Therefore we do not treat it as a systematic error, however we show in Figure 1 the effect of varying the ejected mass between  $5 - 20 M_\odot$ . As can be seen, the effect it weak and shifts the best fit value by roughly  $\pm 10\%$ .

### 3.4. Results and discussion

Our results are summarized in Table 3 and Figures 2—9. We can see that in the case of a RSG ( $n = 3/2$ ), ultraviolet coverage is essential to reduce the statistical uncertainty on the radius. Adding UVOT coverage, even at one day cadence, reduced the statistical uncertainty on the radius from  $\pm 45\%$  to  $\pm 18\%$ . The addition of U-band reduces the uncertainties far less effectively, and U-band photometry is notoriously difficult to calibrate. Therefore our results for U-band are likely over-optimistic. As was observed in Rubin et al. (2016),  $v_{88.5}$  ( $E/M$  in their paper) is statistically well constrained. However, in single bands  $v_{88.5}$  can only be considered a lower limit due to the unknown local host extinction. BVRI coverage was sufficient to constrain the extinction to  $A_V < 0.34$ , and adding UVOT improved these constraints to a range of  $\pm 0.07$  mag. High cadence UV coverage further reduces the uncertainty in  $A_V$  to a range of  $\pm 0.05$  mag.

The results are similar for the BSG ( $n = 3$ ) case. BVRI observations at high cadence are sufficient to reduce the statistical uncertainty on the radius to  $\pm 30\%$ . However, the addition of UVOT or high-cadence UV observations can reduce this uncertainty to  $\pm 10\%$ . Importantly, we could not simultaneously achieve good fits for RSG and BSG models for the same data. In this respect, the models are strongly discriminative.

As was discussed, there are several systematic uncertainties which in some cases are dominant. The dependence on the progenitor's internal structure (via  $f_\rho$ ), and the dependence on the color temperature, although weak, can be significant.

Our conclusions can be summarized as follows:

- Shock-cooling models can discriminate between

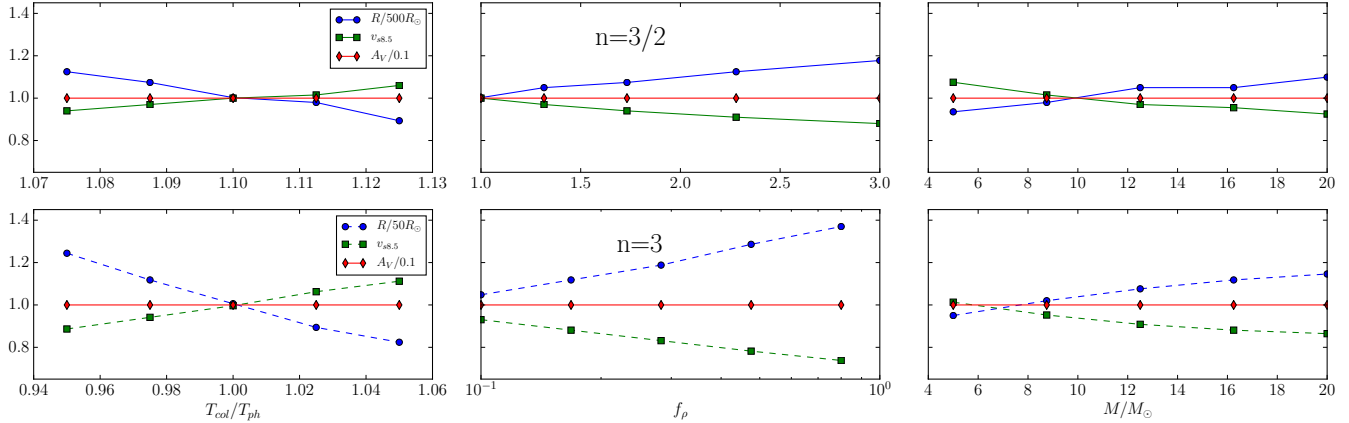


FIG. 1.— Top: systematic dependence of the best fit values for  $R_s$ ,  $v_{s8.5}$ , and  $A_V$  on the unknown parameters  $T_{col}/T_{ph}$ ,  $f_\rho$ , and  $M_{ej}$  for  $n = 3/2$ . Bottom: same for  $n = 3$  with BVRI + SWIFT/UVOT coverage. There is no systematic uncertainty on the extinction. For each case we used the nominal value of two parameters and varied the third.

TABLE 3  
FIT RESULTS FOR SYNTHETIC DATA

	Progenitor	$R_s/R_\odot$	$v_{s8.5}$	$A_V$
True value	RSG	500	1.00	0.10
BVRI	RSG	$465^{+285}_{-155}(\text{stat})^{+117}_{-37}(\text{sys})$	$1.03^{+0.11}_{-0.11}(\text{stat})^{+0.05}_{-0.16}(\text{sys})$	$0.12^{+0.22}_{-0.12}$
UVBRI	RSG	$480^{+243}_{-148}(\text{stat})^{+109}_{-46}(\text{sys})$	$1.00^{+0.09}_{-0.08}(\text{stat})^{+0.06}_{-0.15}(\text{sys})$	$0.08^{+0.17}_{-0.08}$
UVBRI + UVOT	RSG	$504^{+90}_{-88}(\text{stat})^{+153}_{-54}(\text{sys})$	$1.00^{+0.04}_{-0.04}(\text{stat})^{+0.06}_{-0.17}(\text{sys})$	$0.10^{+0.07}_{-0.07}$
UVBRI + ULTRASAT	RSG	$490^{+42}_{-41}(\text{stat})^{+151}_{-46}(\text{sys})$	$1.00^{+0.04}_{-0.04}(\text{stat})^{+0.05}_{-0.17}(\text{sys})$	$0.09^{+0.05}_{-0.05}$
True value	BSG	50	1.00	0.10
BVRI	BSG	$42^{+19}_{-8}(\text{stat})^{+22}_{-1}(\text{sys})$	$1.02^{+0.11}_{-0.10}(\text{stat})^{+0.05}_{-0.36}(\text{sys})$	$0.01^{+0.29}_{-0.01}$
UVBRI	BSG	$45^{+18}_{-5}(\text{stat})^{+23}_{-4}(\text{sys})$	$0.99^{+0.08}_{-0.07}(\text{stat})^{+0.08}_{-0.34}(\text{sys})$	$0.00^{+0.23}_{-0.00}$
UVBRI + UVOT	BSG	$49^{+12}_{-8}(\text{stat})^{+23}_{-8}(\text{sys})$	$1.00^{+0.06}_{-0.05}(\text{stat})^{+0.12}_{-0.33}(\text{sys})$	$0.09^{+0.10}_{-0.09}$
UVBRI + ULTRASAT	BSG	$50^{+7}_{-5}(\text{stat})^{+25}_{-9}(\text{sys})$	$1.00^{+0.05}_{-0.06}(\text{stat})^{+0.11}_{-0.34}(\text{sys})$	$0.10^{+0.07}_{-0.07}$

RSG and BSG progenitors.

- UV coverage reduces the statistical uncertainty on the progenitor’s radius to  $\pm 10\%$ . A huge improvement over current estimates. While this is currently systematics dominated, improved theories and measurements can help to reduce these.
- The addition of UV coverage to measurements in the optical bands allows for the determination of the local host extinction, which is currently challenging to determine.

#### 4. APPLICATION TO KSN 2011A AND KSN 2011D

KSN 2011a and KSN 2011d are two Type II-P SNe recently reported on by Garnavich et al. (2016, G16). The parameters of both SNe are presented in Table 4 (reproduced from G16). G16 analyzed their light curves with RW11 RSG models and reported their best fit parameters to be progenitor radii of  $280 \pm 20 R_\odot$  and  $490 \pm 20 R_\odot$  for KSN 2011a and KSN 2011d respectively, both with explosion energies of  $2 \pm 0.3 \times 10^{51}$  erg (for  $M_{ej} = 15 M_\odot$ ). Their analysis included light curve data until the peak magnitude. G16 concluded that KSN 2011a is not consistent with the simple shock-cooling model, but requires

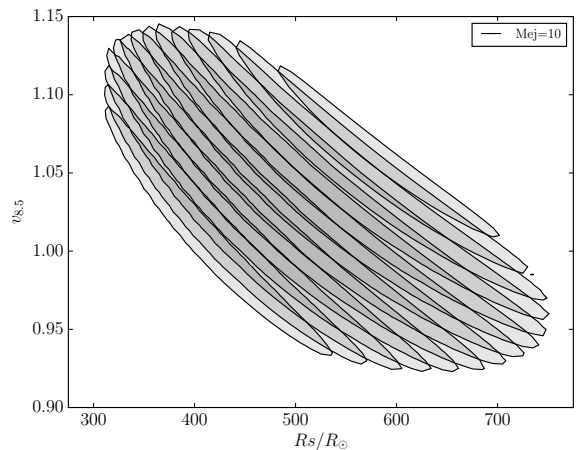


FIG. 2.— Contours showing the critical region of the fit ( $P$ -value  $> 0.05$ ) for RSG with BVRI coverage. The contours represent different values of  $A_V$ .

the shock-breakout to occur from a circumstellar material. This is primarily due to the fast rise observed over a few days. KSN 2011d was well fit by the model, and G16 interpreted an excess at the very early time of the

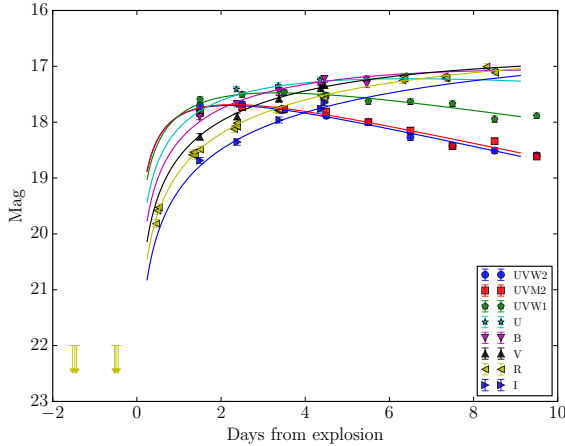


FIG. 3.— Best fit for RSG with UBVRI + UVOT coverage.

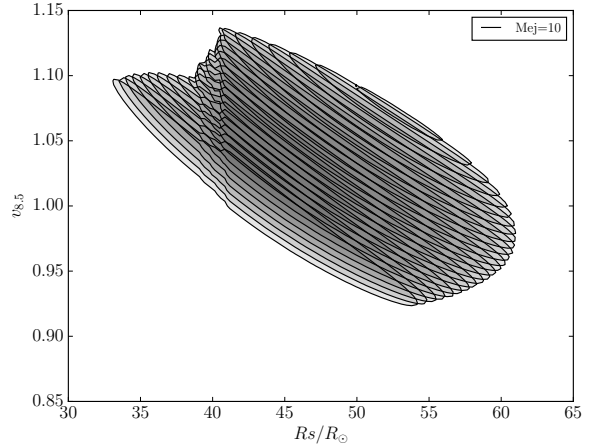


FIG. 6.— Same as Figure 2 for BSG with BVRI coverage.

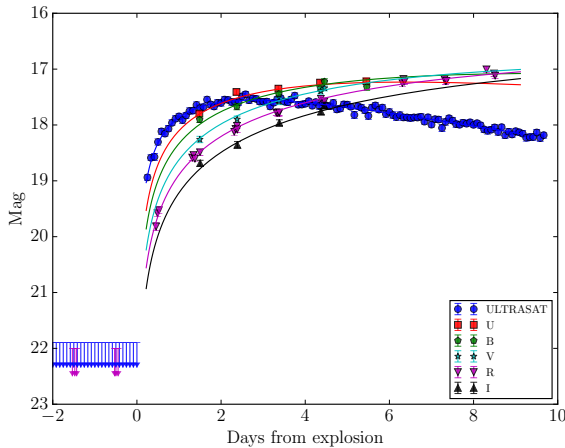


FIG. 4.— Best fit for RSG with UBVRI + ULTRASAT coverage.

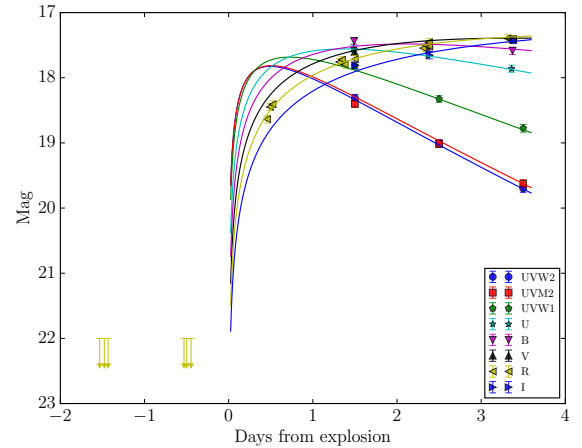


FIG. 7.— Best fit for BSG with UBVRI + UVOT coverage.

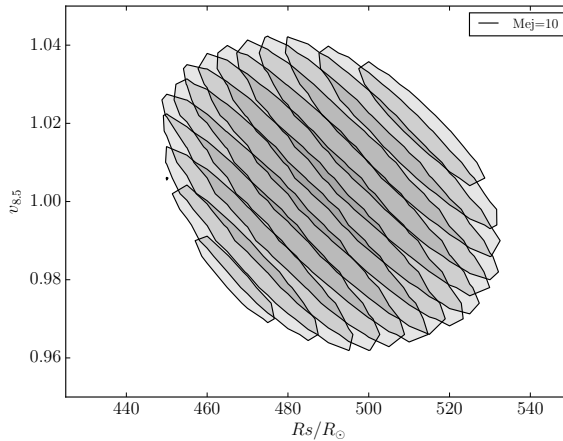


FIG. 5.— Same as Figure 2 for RSG with UBVRI + ULTRASAT coverage.

LC to arise from a shock-breakout. Here we re-analyze the photometry of KSN 2011a and KSN 2011d, taking into account the limitations of validity of the models.

Photometry of KSN 2011a and KSN 2011d were ob-

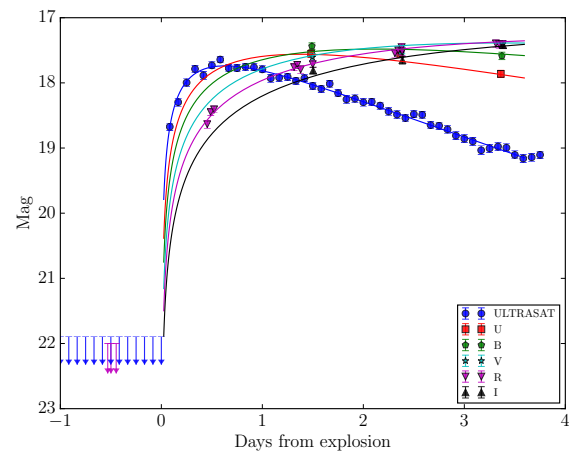


FIG. 8.— Best fit for BSG with UBVRI + ULTRASAT coverage. tained from P. M. Garnavich.<sup>1</sup> We binned the data into 2 hour intervals, taking the errors to be  $\sigma/\sqrt{N-1}$  where  $\sigma$  is the standard deviation and  $N$  is the number of samples

<sup>1</sup> Private communication.

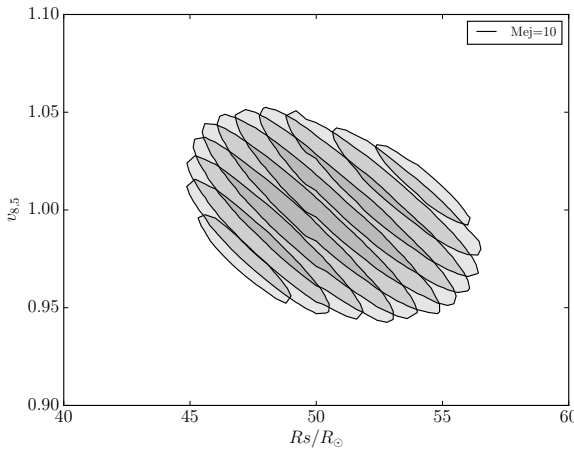


FIG. 9.— Same as Figure 2 for BSG with UBVRI + ULTRASAT coverage.

in the interval. Because only a single band is available for the Kepler SNe, we assumed no host galaxy extinction, and treat our  $v_{88.5}$  as a lower limit (as did G16).

In order to assess G16’s shock-breakout claim, we binned the data to 3.5 hour intervals (same as G16). The model with which G16 compared does not predict what the emission should be prior to breakout. In fact, it is clear from their residual plot that there is correlated excess prior to the points they claim represent the shock-breakout. It is more reasonable to assess whether these points deviate significantly from a smooth function connecting the “pre-” and “post-” breakout. Therefore we fit a 9<sup>th</sup> order polynomial excluding these points, and check the significance of their deviation. G16 binned their data starting from an arbitrary BJD value. We repeat this for seven phases of binning (shifting the binning by a single Kepler point) to see if this is a binning dependent effect.

#### 4.1. Results and discussion

Our results for the fit parameters of KSN 2011a and KSN 2011d are presented in Table 5. We found that KSN 2011a is best fit by a  $n = 3$  model, appropriate for a BSG progenitor. We took  $f_\rho = 0.1$ ,  $\kappa_{0.34} = 1.$ , and  $T_{col} = 1.0$  (see discussion in Section 2 on the choice of parameters). It was necessary to increase the errors by a factor of 3.12 in order to achieve a best fit with  $\chi^2 = 1$ . The best fit is shown in Figure 10. We did not find acceptable fits to  $n = 3/2$  models appropriate for RSGs. We find  $R_s = 10^{+37}_{-7}(\text{stat})^{+8}_{-1}(\text{sys})$  and  $v_{88.5} \geq 4 - 1.8(\text{stat}) - 1.4(\text{sys})$ .<sup>2</sup>

Our result does not agree with that of G16. While they rejected a BSG model due to its fast rise-time, we find that a BSG model is fully consistent with the data. The period of validity in this case is cutoff by the rapid drop in temperature ( $T = 0.7$  eV at 1.7 days for the best fit). Because the cutoff is due to temperature drop (as opposed to the ejecta becoming transparent) there is no strong reason to expect a strong suppression after the cutoff. This result is in tension with the known association of Type II-P SNe with RSG progenitors in pre-explosion imaging (Smartt 2009, 2015), however we find that the model can fit the data self consistently and

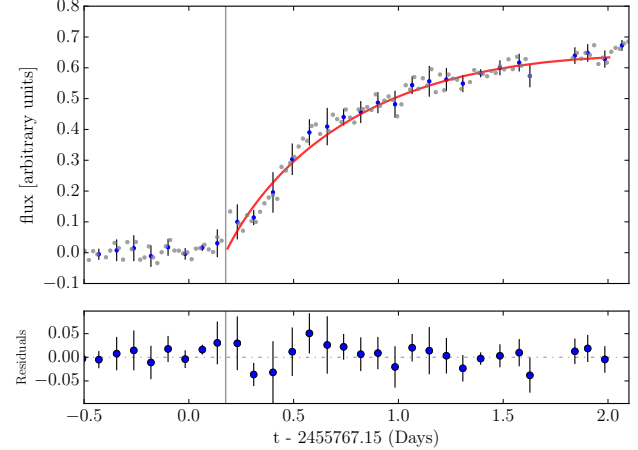


FIG. 10.— Top: best fit to KSN 2011a. Gray points are the original 30 minute cadence data. Blue points are the 2 hour binned data. The gray vertical band in both panels shows the time when the model is not valid between explosion and the beginning of the spherical phase Bottom: residuals.

find no reason to reject the model based on other considerations (e.g. predicted velocities).

KSN 2011d is best fit by an  $n = 3/2$  model, appropriate for a RSG progenitor. We took  $f_\rho = 1$ ,  $\kappa_{0.34} = 1.$ , and  $T_{col} = 1.1$ . It was necessary to increase the errors by a factor of 2.4 in order to achieve any reasonable fits. The best fit is shown in Figure 11. We did not find acceptable fits to  $n = 3$  models appropriate for BSGs. We found that  $R_s = 140^{+91}_{-47}(\text{stat})^{+23}_{-28}(\text{sys})$  and  $v_{88.5} \geq 2 - 0.29(\text{stat}) - 0.19(\text{sys})$ .

Our results again do not agree with those of G16, however the cause is not entirely clear. We too find that an RSG model is in excellent agreement with the data, however our constraint on the radius excludes their best fit value. The peak magnitude of their reported best fit according to RW11 equations 13-14 (despite being beyond the limit of validity) is  $m_{peak} = 20.0$  (including MW extinction), however using the same parameter they calculate it to be  $m_{peak} = 20.23$ . This quarter magnitude discrepancy is the primary source of our conflicting results for the radii.

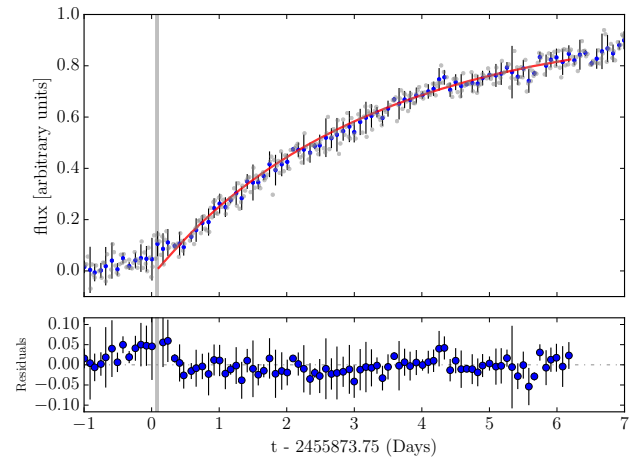


FIG. 11.— Top: best fit to KSN 2011d. Bottom: residuals.

<sup>2</sup> The lower limit is due to the unknown extinction.

TABLE 4  
KEPLER TYPE II-P SUPERNOVA CANDIDATES<sup>a</sup>

Name	Host KIC <sup>b</sup>	SN Type	Redshift (z)	MW A <sub>V</sub> (mag)	Peak Kp <sup>c</sup> (mag)	Date of Breakout (BJD-2454833.0)	Rise Time (days)
KSN 2011a	08480662	II-P	0.051	0.194	19.66±0.03	934.15±0.05	10.5±0.4
KSN 2011d	10649106	II-P	0.087	0.243	20.23±0.04	1040.75±0.05	13.3±0.4

<sup>a</sup> Reproduced from Garnavich et al. (2016)

<sup>b</sup> Kepler Input Catalog (Brown et al. 2011)

<sup>c</sup> Not corrected for extinction

TABLE 5  
FIT RESULTS FOR KSN 2011A AND KSN 2011D.

SN	Progenitor	$R_s/R_\odot$	$v_{s8.5}$	$t_0 - 2454833.0$
KSN 2011a	BSG	$10^{+37(\text{stat})+8(\text{sys})}_{-7(\text{stat})-1(\text{sys})}$	$\geq 4 - 1.8(\text{stat}) - 1.4(\text{sys})$	$934.32^{+0.09}_{-0.16}$
KSN 2011d	RSG	$140^{+91(\text{stat})+23(\text{sys})}_{-47(\text{stat})-28(\text{sys})}$	$\geq 2 - 0.29(\text{stat}) - 0.19(\text{sys})$	$1040.81^{+0.11}_{-0.24}$

In regards to the claim of shock breakout we find that their result is highly dependent on binning and the underlying model. There is no strong prediction for the emission just prior to breakout in any of the NS10/RW11/SW16 models. Therefore the model which G16 used does not fairly test the hypothesis. The approach we explored tests the departure from a smooth function, i.e. a signal indicative of a flash. We present the most and least significant results we obtained given phase shifts (choice of arbitrary BJD values for the first point of the binning) of the 3.5 hour binning. The results are presented in Figure 12 and show that the most significant departure is  $3.85\sigma$ , while the least is just  $1.56\sigma$ . We conclude that their result is not statistically significant, and more events of this nature must be studied.

## 5. CONCLUSIONS

We have explored the uncertainties in applying SW16 shock cooling models to observations. Generating synthetic photometry with a realistic followup campaign and noise model we have shown that ultraviolet coverage is necessary to constrain the progenitors radius in a meaningful way. It is clear that ground-based campaigns will be limited in their ability to constrain the progenitors radius. Shock cooling models are discriminative with regards to the polytropic index. We were unable to self-consistently fit  $n = 3$  models to data generated from  $n = 3/2$  models and vice versa. The uncertainties are strongly influenced by the limits of validity of the models, as was explained in Rubin et al. (2016), although several works have not treated them systematically—leading to incorrect conclusions.

Multi-band light curves have the potential to constrain the local host extinction, with the best performance with high cadence ultraviolet coverage. A dedicated UV satellite such as ULTRASAT (Sagiv et al. 2014) would provide superior coverage even to that which was explored in this work.

We applied our methods to the SN LCs recently published by G16. Our finding do not agree with theirs. First, there is an unknown source of discrepancy of  $\sim 0.25 - 0.5$  magnitudes which we were unable to resolve based on the information provided in their paper. Our estimates of the uncertainties take into account the model’s limitations. We find that a  $n = 3$  model can be self consistently fit to KSN 2011a. This is due in part to the fact that the observed plateau begins after  $T = 0.7$  eV—where the model is no longer valid.

## 6. SUMMARY

- UV coverage at early times is necessary to statistically constrain the progenitor’s radius.
- UV coverage at early times in conjunction with optical bands can provide an accurate measurement of the local host extinction.
- The ejected mass is weakly correlated with  $v_{s8.5}$  and  $R_s$ .

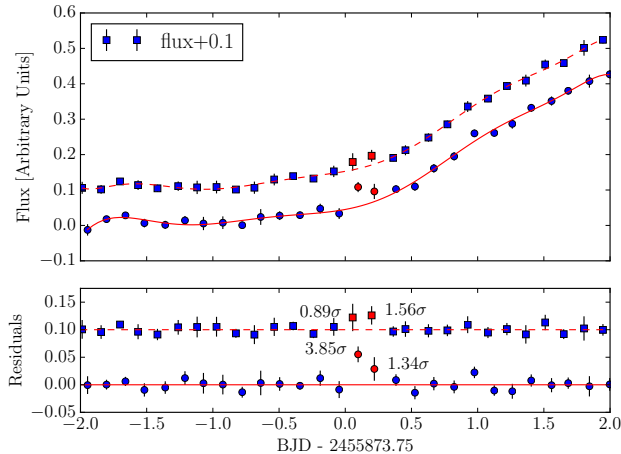


FIG. 12.— Significance of the departure of the shock-breakout identified by G16. Top: the early time light curve binned to 3.5 hour intervals with different binning phases, offset by 0.1 for visual clarity. The data have been fit to a 9th order polynomial (excluding the two points in red) to test departure from a smooth function. Bottom: residuals from the smooth functions. Binning has a dramatic effect on the significance of the departure, which at most is  $3.85\sigma$ , but can drop to  $1.56\sigma$ .

- Both KSN 2011a and KSN 2011d can be self-consistently fit with BSG and RSG shock-cooling models respectively.
- The shock-breakout of KSN 2011d reported by G16 is not statistically significant, and depends strongly on binning effects.

We thank E. Waxman, N. Sapir, and E.O. Ofek for helpful discussions. We thank P. Garnavich for the

Kepler SN data. This research made use of Astropy, a community-developed core Python package for Astronomy (Astropy Collaboration et al. 2013) and the MATLAB package for astronomy and astrophysics (Ofek 2014). AG-Y and AR are supported by the EU/FP7 via ERC grant No. [307260], the Quantum Universe I-Core program by the Israeli Committee for Planning and Budgeting and the ISF; by an ISF grant; by the Israeli ministry of science and the ISA; and by Kimmel and YeS awards.

## REFERENCES

Arcavi, I., Gal-Yam, A., Yaron, O., et al. 2011, *ApJL*, 742, L18  
 Arcavi, I., Hosseinzadeh, G., Brown, P. J., et al. 2016, ArXiv e-prints  
 Astropy Collaboration, Robitaille, T. P., Tollerud, E. J., et al. 2013, *A&A*, 558, A33  
 Bessell, M. S. 1990, *PASP*, 102, 1181  
 Bose, S., Valenti, S., Misra, K., et al. 2015, *MNRAS*, 450, 2373  
 Brown, T. M., Latham, D. W., Everett, M. E., & Esquerdo, G. A. 2011, *AJ*, 142, 112  
 Cardelli, J. A., Clayton, G. C., & Mathis, J. S. 1989, *The Astrophysical Journal*, 345, 245  
 Ergon, M., Sollerman, J., Fraser, M., et al. 2014, *Astronomy and Astrophysics*, 562, doi:10.1051/0004-6361/201321850  
 Gal-Yam, A., Kasliwal, M. M., Arcavi, I., et al. 2011, *ApJ*, 736, 159  
 Gall, E. E. E., Polshaw, J., Kotak, R., et al. 2015, *A&A*, 582, A3  
 Garnavich, P. M., Tucker, B. E., Rest, A., et al. 2016, *ApJ*, 820, 23  
 Gezari, S., Dessart, L., Basa, S., et al. 2008, *ApJL*, 683, L131  
 González-Gaitán, S., Tominaga, N., Molina, J., et al. 2015, *MNRAS*, 451, 2212  
 Kaiser, N., Aussel, H., Burke, B. E., et al. 2002, in *Proc. of SPIE*, Vol. 4836 (SPIE), 154–164  
 Kulkarni, S. R. 2013, *ATel*, 4807, 1  
 Law, N. M., Kulkarni, S. R., Dekany, R. G., et al. 2009, *PASP*, 121, 1395  
 Nakar, E., & Sari, R. 2010, *ApJ*, 725, 904  
 Ofek, E. O. 2014, *Astrophysics Source Code Library*, 1407.005  
 Pastorello, A., Sauer, D., Taubenberger, S., et al. 2006, *MNRAS*, 370, 1752  
 Planck Collaboration, Ade, P. A. R., Aghanim, N., et al. 2015, arXiv:1502.01589  
 Quimby, R. M., Wheeler, J. C., Höflich, P., et al. 2007, *The Astrophysical Journal*, 666, doi:10.1086/520532  
 Rabinak, I., & Waxman, E. 2011, *ApJ*, 728, 63  
 Rubin, A., Gal-Yam, A., Cia, A. D., et al. 2016, *ApJ*, 820, 33  
 Sagiv, I., Gal-Yam, A., Ofek, E. O., et al. 2014, *AJ*, 147, 79  
 Sapir, N., & Waxman, E. 2016, arXiv:1607.03700 [astro-ph], arXiv: 1607.03700  
 Schawinski, K., Justham, S., Wolf, C., et al. 2008, *Science*, 321, 223  
 Shussman, T., Waldman, R., & Nakar, E. 2016, arXiv:1610.05323 [astro-ph], arXiv: 1610.05323  
 Smartt, S. J. 2009, *ARA&A*, 47, 63  
 —. 2015, *PASA*, 32, e016  
 Tartaglia, L., Fraser, M., Sand, D. J., et al. 2016, ArXiv e-prints  
 Valenti, S., Sand, D., Pastorello, A., et al. 2014, *MNRAS*, 438, L101  
 Valenti, S., Howell, D. A., Stritzinger, M. D., et al. 2016, *MNRAS*, 459, 3939  
 Waxman, E., Mészáros, P., & Campana, S. 2007, *ApJ*, 667, 351